HEAT TRANSFER AND STABILITY FOR A MOVING COOLANT EVAPORATING IN A POROUS CERMET

V. A. Maiorov and L. L. Vasil'ev

UDC 532.685:536.24

Transpiration cooling takes on some new features if a liquid coolant is employed that evaporates within the pores; the cooling is markedly enhanced by the latent heat of evaporation, while the heat transfer within the porous material is very rapid, and the volume of liquid required is small. Also, low temperatures (including cryogenic ones) can be obtained.

The main principles of the method were known 40 years ago (see [1, 44] for the early years), but extensive use of the technique was delayed until recently even for compact heat exchangers on account of the very considerable complexity and instability of the processes.

Physical and Analytical Models. Figure 1 shows models [2, 3] for evaporative liquid transpiration cooling; the liquid coolant at an initial temperature t_0 is forced by the pressure difference $P_0 - P_1$ through the heated porous wall. The pressure falls as the liquid moves while the temperature rises; at some distance L from the inlet, the saturation state is attained, which is followed by gradual evaporation over the length LK and displacement of the superheated vapor over the part $K\delta$ within the porous plate.

There are thus three regions of motion (liquid, two-phase, and vapor), whose boundaries are unknown and have to be determined. The conditions for thermodynamic equilibrium may be met at the boundaries, or (in the more general case) the conditions for thermodynamic disequilibrium between the temperature and pressure of the coolant.

Various assumptions are made by the treatment: the process is one-dimensional and stationary, the physical parameters of the porous material are constant, the enthalpy of the coolant at the start is equal to that of the liquid, while the enthalpy at the end of the evaporation region is that of the saturated vapor at pressure P_l at the start of the evaporation region, the homogeneous two-phase flow in the evaporation region has the constant saturation temperature $t_s(P_l)$ occurring at the start of the evaporation region, the physical parameters of the liquid and vapor phases of the coolant are constant and correspond to saturation at the pressure P_1 of the surrounding medium, the heat transfer by conduction through the coolant is negligible, the capillary pressure in the evaporation region is small by comparison with the total pressure difference across the plate, and the coolant flow rate does not exceed the critical value.

The model of Fig. 1a is then described by the following equations:

1) equation of continuity

$$G = \text{const}; \tag{1}$$

2) equation of motion for the single-phase coolant in the porous material, viz., a modified Darcy equation:

$$-\frac{dP}{dZ} = \alpha\mu v G + \beta v G^2; \tag{2}$$

3) heat-conduction equation in the evaporation reqion:

$$\lambda\frac{d^2T_2}{dZ^2} = h_v(T_2 - t_2) = G\frac{di}{dZ}; \tag{3}$$

4) equations describing the distributions of the temperatures T_j of the material and t_j of the coolant in the regions of single-phase flow:

$$\lambda\frac{d^2T_j}{dZ^2} = h_v(T_j - t_j); \tag{4}$$

A. V. Lykov Institute of Heat and Mass Transfer, Academy of Sciences of the Belorussian SSR, Minsk. Novopolotsk Polytechnical Institute. Translated from Inzhenerno-Fizicheskii Zhurnal, Vol. 36, No. 5, pp. 912-934, May, 1979. Original article submitted November 2, 1978.

0022-0841/79/3605-0611$07.50

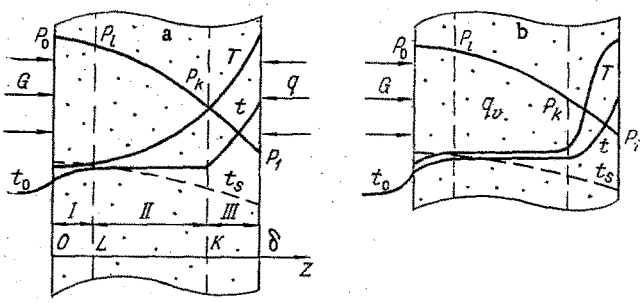

Fig. 1. Models: a) with external heat input [2]; b) with bulk heat production [3]; I) liquid flow; II) evaporation region; III) vapor flow.

$$Gc_j \frac{dT_j}{dZ} = h_v (T_j - t_j); \tag{5}$$

5) dimensionless equation for convective heat transfer in the single-phase coolant within the material:

$$\mathrm{Nu}_j = 3.5 \cdot 10^{-3} \mathrm{Re}_j \mathrm{Pr}_j; \quad \mathrm{Nu}_j = \frac{h_v (\beta/\alpha)^2}{\lambda_j}; \quad \mathrm{Re}_j = \frac{G(\beta/\alpha)}{\mu_j} \tag{6}$$

subject to the boundary conditions

$$Z = L \quad t_1 = t_2 = t_s(P_l); \quad T_1 - t_1 = T_2 - t_2 = \Delta T_1;$$
$$\lambda \frac{dT_1}{dZ} = \lambda \frac{dT_2}{dZ} = G[i'(P_l) - ct_0]; \tag{7}$$

$$Z = K \quad t_2 = t_3 = t_s(P_l); \quad T_2 = T_3; \quad \lambda \frac{dT_2}{dZ} = \lambda \frac{dT_3}{dZ} = G[i''(P_l) - ct_0]; \tag{8}$$

$$Z = \delta \quad P = P_1; \quad T_3 \leqslant T^{**}. \tag{9}$$

Here G is the specific mass flow rate; α and β, viscosity and inertial coefficients representing the resistance of the porous material; v, specific volume; h_V, volume expansion coefficient; T**, maximum permissible temperature for the porous material; $T_j = T_1$; $t_j = t_1$; $c_j = c'$; $\mathrm{Pr}_j = \mathrm{Pr}'$; $\lambda_j = \lambda'$; $\mu_j = \mu'$ over the liquid part of the path ($0 < Z < L$) and $T_j = T_3$; $t_j = t_3$; $c_j = c''$; $\mathrm{Pr}_j = \mathrm{Pr}''$; $\lambda_j = \lambda''$; $\mu_j = \mu''$ on the vapor part ($K < Z < \delta$); further, single and double primes relate to the parameters of the liquid and vapor in the state of saturation at pressure P_1.

A similar model has been used for the cooling of a porous heat-producing rod [3].

If the thermal conductivity of the porous material is comparable with that of the coolant (e.g., combination of porous ceramic with a liquid or of porous metal with a liquid-metal coolant), one has to incorporate the heat transfer by conduction through the coolant. Then (5) is replaced by

$$\Pi\lambda_j \frac{d^2 t_j}{dZ^2} + h_v (T_j - t_j) = Gc_j \frac{dt_j}{dZ}, \tag{10}$$

where Π is the porosity of the material.

The frictional resistance for a two-phase flow has been calculated [2, 3] for a homogeneous model, on the basis of (2), in which the physical parameters of the mixture dependent on the mass content x of the vapor are substituted into (2). The specific volume is uniquely related to the latter quantity:

$$v = v' + x(v'' - v'), \tag{11}$$

while the following expressions define the effects of the kinematic viscosity ν = μv on the final results:

$$\nu_I = \nu' + x(\nu'' - \nu'); \tag{12}$$

$$\nu_{II} = [\mu' + x(\mu'' - \mu')][v' + x(v'' - v')]. \quad (13)$$

Therefore, this transpiration cooling involves a variety of largely unexamined problems:

1) laws of resistance and heat transfer for a single-phase coolant moving in a porous cermet;

2) thermophysical parameters of porous materials;

3) detailed mechanism and the resistance and heat-transfer laws for a two-phase flow in such a material; and

4) stability of the evaporative cooling.

The general position becomes clear if one bears in mind that even the relatively simple case of gas transpiration cooling is a relatively new division of heat transfer that is only now beginning to develop; data are being accumulated on the first two of the above problems. See [4] for a fairly detailed survey of the available data on resistance, heat transfer, flow effects, and the influence of gas compressibility for a one-phase coolant moving in a porous cermet, including results on stability for gas transpiration cooling. To a first approximation, we can assume that the heat transfer for a single-phase coolant in a porous metal has been examined in some detail, and in particular that (6) represents a generalization of equations derived when the parameter β/α is used as the characteristic dimension of the porous structure.

Measurements on Liquid Transpiration Cooling. Very few detailed results have so far been obtained on the mechanisms and quantitative characteristics of the heat transfer and resistance under these circumstances, especially as regards the stability; the main reason is that the various problems are very closely related, since measurements can be made on the evaporation mechanism only for a stable system, while one can create a stable system only if the resistance and heat-transfer laws are known. The instabilities encountered in the early experiments discouraged research for a long period. Also, there are major difficulties in researching evaporation in a porous material, and this applies to many such studies on such materials.

Table 1 collects the available evidence on the conditions used in experiments; although it might appear that there is an abundance of papers, it has not proved possible to extract any major data on the evaporation mechanism. There are many reasons for this. For example, the major efforts were directed elsewhere in various studies. An instance is that of [9, 18], where measurements were made on the effects of coolant injection on the external convective heat transfer. In [42] there was an excess flow of collant designed to produce film cooling on the porous wall of the combustion chamber of a liquid-fueled rocket motor, as well as on the latter part of the solid nozzle wall. It is also widely assumed that there is a critical coolant flow rate above which the temperature of the outer surface of the porous wall remains near or below the saturation temperature of the coolant, whereas at lower flow rates the surface temperature rises rapidly and fluctuations in temperature, pressure, and flow rate begin to appear [6, 8, 9, 18]. In every case, the experiments were halted when the evaporation region receded into the porous wall. There is also a restricted group of papers [7, 10, 11-13, 14-17, 19] in which the evaporation was allowed to extend to some distance within the wall, although the coolant flow pattern was examined visibly only in [7, 15, 17].

The most detailed studies on the evaporation mechanism in a porous heat-producing material appeared to be those of [15]; three distinct ranges occur in the relation between the outer surface temperature and the coolant flow rate for a constant rate of heat production in the wall (Fig. 2a).

In region I (high mass flow rates) there is single-phase flow, and the temperature of the outer surface and the temperature of the liquid on emergence are below the saturation point, although the latter is approached as the flow rate is reduced.

In region II a liquid–vapor mixture emerges from the wall; the hydraulic resistance increases as the proportion of vapor rises, and premature damage may be prevented and the flow rate may be controlled by doubling the initial pressure difference. The temperature of the two-phase mixture at the outlet remains constant at the saturation temperature. The point of onset of evaporation moves into the wall as the flow rate falls.

The temperature of the outer surface then exceeds the saturation temperature by not more than 3-10°C for bulk heat-production rates in the range $q_V = (4.5\text{-}14) \cdot 10^8$ W/m^3.

TABLE 1. Working Conditions in Liquid Transpiration Cooling

Form of heating	Heat load q, W/m²; q_V, W/m³	Coolant flow rate G, kg/m²·sec	Pressure difference across wall P_0-P_1, bar	Shape and size of porous wall d, L, mm	Thickness δ of porous wall, mm	One-layer wall	Multi-layer wall	Porous material	Porosity π	Maximum temp. T in stable state, °C	Ref.
Convective	$q\approx(1,0-2,5)\cdot10^4$	0,005—0,014	0,7	Circular disk d=25,4	12,7	×		Bronze	0,26	102	[5]
Convective	$q\approx1,4\cdot10^6$	—	—	Circular cylinder $d=25,4$; $L=38$	10,0	×		Stainless steel; nickel	—	—	[6]
Convective	$q\approx2,8\cdot10^5$	0,055	1,0	Square plate 50,8×50,8	3,18	×		Rigimesh	—	107	[7]
Convective	—	1,0—10,0	—	Circular disk $d=10$	8,0	×		Steel	—	360	[8]
Convective	$q\approx(1-2)\cdot10^4$	—	0,04—0,20	Rectangular plate 280×130	10,0	×		Copper	0,35	110	[9]
Radiation-convective	$q=(0,7-2,8)\cdot10^5$	0,013—0,092	0,5—1,0	Circular disk $d=76$	7,0		×	Rigimesh+Refrasil	0,20	1070	[10]
Ohmic	$q_v\approx(1-3)\cdot10^8$	0,04—0,24	0,003—0,070	Square plate 45×45	0,33; 3,53	×	×	Rigimesh+ Stainless steel	—	140	[11]—[13]
Radiation	$q=1,5\cdot10^5$	0,033—0,050	—	Circular disk $d=102$	12,7	×	×	Stainless steel +Q-felt	0,53; 0,77	1090	[14]
Ohmic	$q_v=5\cdot10^8$ $q_v=7\cdot10^8$ $q_v=14\cdot10^8$	0,5—2,0	—	Rectangular plate 210×33	5,0; 1,4; 0,5	×		Nichrome	0,40; 0,32; 0,25	125	[15]
Radiation	$q=(2,3-5,7)\cdot10^5$	—	—	Circular disk $d=50,8$	5,0		×	Stainless steel +Refrasil	0,10	830	[16]
Convective	$q\approx6,75\cdot10^5$	0,14	2,0	Circular cylinder $d=150$; $L=600$	10,0		×	Stainless steel+Refrasil	0,10	900	[16]
Radiation	$q=(1,1-2,1)\cdot10^5$	0,020—0,057	0,01—0,03	Circular disk $d=28,8$; $d=35,2$	3,3; 5,4	×		Rigimesh	0,17; 0,25	160	[17]
Convective	$q\approx(1-3)\cdot10^4$	0,001—0,010	0,05	Rectangular plate 300×30	10,0	×		Copper	0,33; 0,41	180	[18]
Convective	$q\approx(1-2)\cdot10^6$	0,5—2,0	—	Circular cylinder $d=40$; $L=40$	2,5	×		Nichrome	0,25	700	[19]
Convective	$q=(1-2)\cdot10^6$	2,0—10,0	—	Circular cylinder $d=127$; $L=60$	12,7	×		Copper; bronze	0,50	110	[42]

Notes: 1) The coolant in all studies apart from [11-13] was water, while in [11-13] it was liquid nitrogen; 2. External pressure atmospheric in all cases apart from [11-13, 42]; vacuum was used in [11-13], while $P_1 \approx 20$ bar in [42] in the combustion chamber of the liquid rocket motor.

In region III a two-phase mixture emerges from the wall, which is a flow of vapor containing drops of liquid; the uneven permeability of the plate causes the onset of evaporation to occur in places at the inner surface, which is accompanied by local boiling, with consequent fluctuations in pressure and flow rate. The wall temperature then rises rapidly on account of inadequate cooling. This mode does not allow of calculation.

Much larger rises in the outside surface temperature were observed [19] in convective heating of the wall (Fig. 2b). Here the temperature of the outside surface rose sharply to 700°C on going from region I to region II.

Therefore, in bulk heat production [15] and in external convective heating [19] it has not proved possible to produce conditions under which the two-phase flow evaporates completely within the porous material and the coolant escapes as superheated vapor while the region of onset of boiling lies within the porous wall. In [15] stable conditions were produced only with a two-phase mixture with a vapor content not more than 40% by mass. One of the reasons for this was the small thickness of the porous nichrome wall: δ = 0.5, 1.4, and 5 mm in bulk heat production, or δ = 2.5 mm in convective heating. In these systems, the extent of the evaporation range was greater than the wall thickness. Also, inhomogeneity in the material had a marked adverse effect on the results.

Figures 2b and 3 show clearly that higher heat inputs cause a marked rise in the surface temperature (Fig. 3) and ultimately a jump in the surface temperature (Fig. 2b) as a region of onset of evaporation penetrates into the wall. In the case of Fig. 3, the rise in surface temperature was restricted by the temperature of the external flow.

Detailed visual observations were reported in [17]; the basic working conditions in a system with radiative heating was chosen such that the coolant began to boil on the inner surface of the wall. The escaping vapor was accompanied by minute droplets of liquid. Under these conditions, there were frequently pressure fluctuations in the system. Visual examination showed that the pressure increased when vapor bubbles appeared and grew on the inner surface. The pressure then fell sharply as the bubbles collapsed into the porous wall, and the process repeated with a period of about 6 min.

A somewhat different picture of the completion of evaporation was observed in [7]; here a boiling film evaporated. Areas of dry surface were exposed as the flow rate was reduced, but there were no pressure fluctuations in the system.

Stability in Transpiration Cooling. Instability is the most undesirable and hazardous aspect of transpiration cooling; such a system is aperiodically unstable (particularly in evaporative transpiration), since some slight deviation from the steady state results in the absence of any other nearby steady state, and large monotone variations can occur.

The instability in evaporative cooling does not allow one to stabilize the position of the evaporation region within the porous material. It has been found [14] that minor variations in the process parameters result in uncontrollable displacement of the onset of evaporation from the outer surface to the inner one, which is accompanied by change in the liquid flow conditions, with superheated vapor emerging in some areas. If the heat loading is heavy, this can result in damage to the porous wall, while at low heat loads there is a considerable rise in the temperature of the outer surface, which is followed by oscillation.

Figure 4 shows the data of [17], which indicate the temperature variation during gradual spontaneous movement of the start of evaporation towards the inner surface (as governed by equations (1) and (2)) and emergence on the inner surface as given by (3) for moderate external heat input. Table 2 gives the working parameters and the calculated results, where τ is the time from the start of heating. The coolant flow rate was kept constant. The latter condition was the basic one for operation with this equipment, namely with boiling at the inner surface. The density of the external heat flux used in the calculation was about 66% of the observed value (the experiments showed that only 60-80% of the incident radiation flux was absorbed by the outer porous surface).

The physical nature of the instability in [16, 23] is that the resistance of the porous material to the flow of vapor is very much greater than that to the flow of liquid, so any slight shift in the position of evaporation within the material causes an appreciable change in the resistance, and this causes a substantial change in the flow rate for a constant pressure difference. This can continue until the point of onset of evaporation lies outside the porous material.

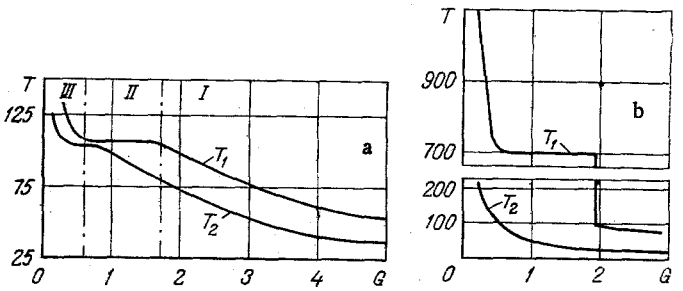

Fig. 2

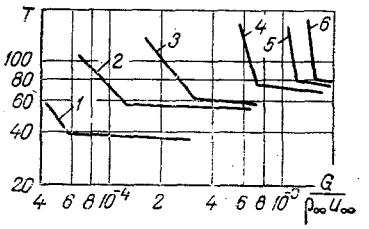

Fig. 3

Fig. 2. Temperatures T_1 and T_2 of the outer and inner surfaces of a porous wall in relation to coolant flow rate: a) with bulk heat production [15] for δ = 1.4 mm, $q_V = 4.5 \cdot 10^8$ W/m^3; b) with external heat input [19] for δ = 2.5 mm; T, °C; G, kg/m^2·sec.

Fig. 3. Effects of temperature t_∞ of a gas flow of constant speed u_∞ = 10 m/sec on the temperature of the outer surface of a porous wall in relation to the relative coolant flow rate $G/\rho_\infty u_\infty$ [18]: 1) t_∞ = 100°C; 2) 200; 3) 300; 4) 400; 5) 500; 6) 600.

These physical arguments have been used in a method of improving the stability by means of an additional internal layer of porous material having a higher resistance. This sets up a large pressure difference, and consequently the resistance change due to displacement of the evaporation region within the outer layer is comparatively slight and does not affect the flow rate appreciably. Implementation of this idea has provided a stable system [10, 16].

Figures 5 and 6 show some experimental data [10, 16] in which a system with this type of design was used, in which there were outer and inner cermet porous walls with insulating material between. Stable evaporation occurred in the insulating layer. A narrower definition of stability was used in [10], which applied only for efficient use of the coolant (production of superheated vapor), so the stable emergence of a two-phase mixture in Fig. 5 was termed metastable, since the apparatus could work for a long period in this state.

It was also pointed out [10] that the considerable pressure difference across the inner layer not only provides conditions for good flow-rate control but also suppresses inhomogeneity in the coolant flow arising from gravitational forces and accelerations occurring in the inhomogeneous porous structure, along with any effects from nonuniform distribution of the external pressure and possible pressure pulsations arising from evaporation within the porous structure. The large pressure difference also reduces the evaporation thickness on account of the more rapid decrease in the saturation temperature and the increase in the superheating of the two-phase mixture.

The results of [17] are of interest, since they relate to a very small pressure difference across the wall: $P_0 - P_1$ = 0.01-0.03 bar. The inhomogeneity of the wall is very prominent in this case, and this can often lead to local breakthrough of liquid jets. Moreover, the pressure difference across the wall was comparable with the capillary pressure $\Delta P = 2\sigma/r$, and the data may be processed in terms of the dimensionless parameter $R = r\delta(\alpha\mu vG + \beta vG^2)/2\sigma$, namely the ratio of the pressure difference across the wall to the capillary pressure, to show that the stable states correspond to $R > 1$ and the unstable ones to $R < 1$. This means that even capillary forces can be a cause of instability in the capillary region if the pressure difference is so small as to be comparable with the capillary pressure.

Thermal protection by transpiration is best performed with a two-layer wall [10, 23]; the inner layer is of low porosity and constitutes the load-bearing part of the structure, so the pressure difference across this is sufficient to ensure efficient control. The outer protective layer is a heat-resistant material of high porosity and low thermal conductivity, which is also chemically inert to the coolant and to the external flow. This protects the inner layer from the high temperature and provides the conditions for complete evaporation and for superheating of the resulting vapor.

Improved stability due to an inert layer has also been observed in transpiration cooling in the presence of bulk heat production [11]; recent studies [12, 13] have dealt with the effect on the stability, from the thickness, porosity, and material of this layer. The most

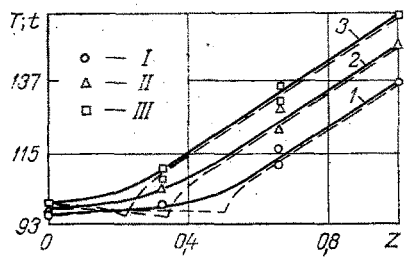

Fig. 4

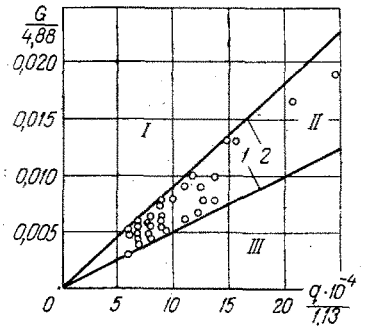

Fig. 5

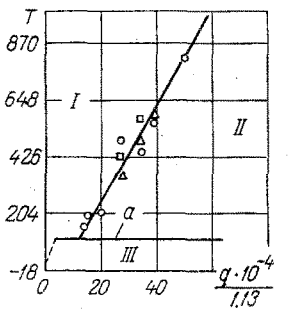

Fig. 6

Fig. 4. Changes in temperature distribution in porous material (solid lines) and in coolant (broken lines) as point of onset of evaporation approaches the inner surface of a porous wall [17]; for explanation see Table 2.

Fig. 5. Flow rate for water in relation to density of absorbed external heat flux in the stable state [10]: I) metastable range; II) stable range; III) unstable range with rapid wall superheating; 1) superheated steam, 1090°C; 2) dry saturated steam, 100°C; G/4.88, kg/m²·sec; $q \cdot 10^{-4}/1.13$, W/m².

Fig. 6. Temperature of outer surface as a function of heat-flux density in the stable state [16]: I, III) unstable regions; II) stable region; *a*) saturation temperature.

TABLE 2. Data of [17] from Fig. 4

Parameters	Theoretical results			Observed results		
	1	*2*	*3*	*I*	*II*	*III*
τ, min	—	—	—	7,0	11,5	17,5
$\frac{G \cdot 10^3}{4,88}$, $\frac{kg}{m^2 \cdot sec}$	9,38	9,38	9,38	9,38	9,38	9,38
$\frac{q \cdot 10^{-4}}{1,13}$, $\frac{W}{m^2}$	10,71	10,81	10,87	16,25	16,25	16,25
$\frac{(P_0 - P_I) \cdot 10^3}{2,54}$, bar	0,15	0,07	0,00	—	—	—
$\frac{(P_I - P_k) \cdot 10^3}{2,54}$, bar	19,87	20,06	20,06	—	—	—
$\frac{(P_k - P_1) \cdot 10^3}{2,54}$, bar	59,41	84,10	107,48	—	—	—
$\frac{(P_0 - P_1) \cdot 10^3}{2,54}$, bar	79,44	104,22	128,14	11,20	8,20	7,40

important result is that it was possible to make a stable system consisting of a porous heated plate of thickness 0.33 mm and an additional unheated plate of stainless steel of thickness 3.2 mm. The start of the evaporation zone lay within the additional plate, while superheated vapor emerged from the heated one. However, the general design is closer to that of a transpiration system with external heat input.

The above shows that the additional internal layer of elevated resistance stabilizes evaporative cooling; this was an experimental discovery, but for a long time it lacked an appropriate theoretical explanation that would enable one to define the optimum combination of parameters for the two layers.

Analytical Examination of Evaporative Cooling in a Porous Wall with External Heat Input. The first theoretical studies [14, 24] were very similar in formulation and in results. Identical models were used, which involved assumptions on local equilibrium (T = t) between the coolant and the porous material and on the thickness K − L → 0 of the evaporation zone (here and subsequently, the models are as referred to in Fig. 1). Only the thermal state of the system was examined in both instances.

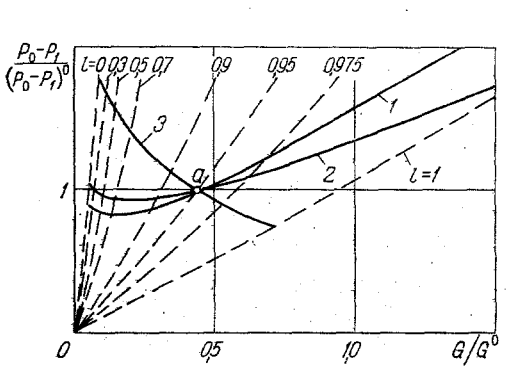

Fig. 7

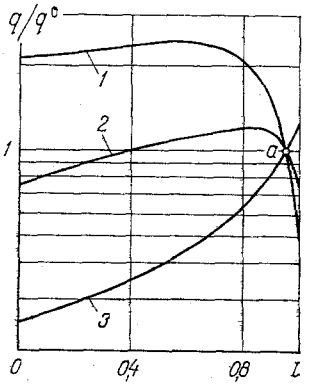

Fig. 8

Fig. 7. Hydrodynamic characteristics of an evaporative cooling system [32].

Fig. 8. Thermal characteristics of an evaporative cooling system [32].

The next advance in the analysis was incorporation of the temperature difference between the porous material and the coolant ($T \neq t$) along with the finite thickness of the evaporation zone $K - L \neq 0$ [25-27]. A deficiency of these studies was that the point of onset of evaporation was determined from the condition that the coolant temperature equals the saturation temperature t_s, which was constant. Numerical calculations have been performed [26] on the thickness of the evaporation zone in relation to the external pressure, the physical parameters of the coolant (N_2O_4, NH_3), the surface area available for internal convective heat transfer, the input heat flux density, and the thermal conductivity of the porous material. These calculations were performed for parameters typical of combustion chambers and nozzles in liquid rocket engines.

The motion of the coolant evaporating within a flat porous wall has been examined [28, 29] on the assumption that the evaporation zone is thin; the thermal and hydrodynamic aspects of the process were combined [28, 30] to demonstrate the scope for instability. Here it was assumed that the temperature of the coolant was equal to that of the porous material. Another study similar to [28] was for a cylindrical wall [31]. A preliminary stability condition has also been formulated [30]. Careful studies have been performed [32, 33] on stability in a model with an infinitely thin evaporation zone and local thermal equilibrium between the porous material and the coolant. Results from the thermal and hydrodynamic treatments were combined in the full characterization; the hydrodynamic characteristics relate the coolant flow rate to the pressure difference across the wall for a constant external heat input. The thermal characteristics relate the external heat-flux density to the coordinate of the phase-transition surface for a constant pressure difference. Figures 7 and 8 show examples of these characteristics.

These characteristics also define the stability condition. It was shown that evaporation cooling with external input is stable if the working point lies on the rising branch of the hydrodynamic characteristic (for independent change in the pressure difference):

$$\frac{d\Delta P}{dG} > 0 \tag{14}$$

or on the falling part of the thermal characteristic (for independent change in the external heat flux density):

$$\frac{dq}{dl} < 0. \tag{15}$$

Point a in Figs. 7 and 8 corresponds to systems 1 and 2 stable, while system 3 is unstable. An important point is that the results on the stability given by the two types of characteristic were identical.

The stability conditions have been used [33] with the condition for absence of wall burn in analytic expressions for the parameters of the stable (safe) operating conditions. It was found that the stability condition imposes very severe restrictions on the system parameters,

and any deviation from these constitutes one of the major reasons for the instability so frequently described in experiments. The physical cause of these severe restrictions is the sharp fall in coolant flow rate when the evaporation zone penetrates into the plate.

A method has been examined [34] for improving the stability by means of an additional inert porous layer. Studies were performed on the motion of the coolant evaporated in the outer layer of a two-layer porous plate. It was shown that such a plate provides improved stability. The structural and thermophysical characteristics of both layers were determined subject to absolute stability in the system as a whole, i.e., stability for any position of the evaporation surface within the outer layer.

The model of Fig. 1a, which is described by (1)-(9), has been used [2] to examine the effects of the finite evaporation thickness on the motion of the coolant. In particular, the following characteristics were defined: the relative scales of the various coolant flow ranges, the relative pressure differences over each of these ranges, the importance of the evaporation region in the total resistance, and the effects of the bulk heat-production rate in the evaporation region.

Analytical Study of Evaporative Cooling for a Porous Body with Bulk Heat Production. Several papers [3, 35-38, 43] deal in detail with evaporative cooling for porous fuel rods; fairly good physical and analytical models (Fig. 1b) have been employed [3]. A logical calculation sequence was used for the heat transfer, resistance, and stability. There are also other analytical studies [35, 36] on the motion of the evaporating coolant and on the temperature pattern.

Hydrodynamic and thermal characteristics have been constructed [37], and these provide a basis for analysis for aperiodic stability; this approach has given the acceptable pressure fluctuations in a stable system for a porous rod, as well as the permissible fluctuations in bulk heat production.

The particular significance of these characteristics will be clear from the complexity of measurements on the resistance and heat transfer for two-phase flows in porous materials. The trends can be established only from resultant effects within the porous structure. The hydrodynamic and thermal characteristics are integral ones that can be constructed from measurements, at least as regards the part corresponding to the region of stable and safe operation. The observed characteristics can be compared with theoretical ones to define many features of the process.

The method of improving the stability with two-layer components has been analyzed [38]; conclusions were drawn on the motion of a coolant evaporating within the outer layer in a two-layer porous rod, and it was shown that the stability is enhanced by increasing the relative resistance of the inner layer.

Analytical expressions have been derived [43] for the structural characteristics of porous layers, particularly those providing absolute stability.

Other studies [39, 40] somewhat later than [3, 35] also dealt with the theory of evaporation cooling for porous rods, but a very highly simplified model was used, since only viscous flow of the coolant was considered, while the coolant and porous material were taken as identical in temperature. The most serious deficiency of this analysis was that the pressure in the evaporation zone was assumed constant, i.e., the pressure drop across this zone was neglected. As a result, [40] gave dubious conclusions, in particular that the coolant flow rate increases as the evaporation zone penetrates into the material.

Comparison of Theory with Experiment. The heat-transfer rate and the resistance in the evaporation zone dominate evaporative cooling; quantitative characteristics can be defined only by careful comparison of theory and experiment. However, no such comparison has yet been performed, and therefore the available experimental evidence quoted above is not supported by even preliminary theoretical analysis, since instead more restricted purposes were served by the studies, viz., definition of the major features of the process and testing of design viability. It is therefore difficult to extract any information on the heat-transfer rates and resistance in the evaporation region.

It has been observed [26] that satisfactory agreement between the theoretical and observed temperature distributions within a liquid-fueled rocket motor nozzle cooled by N_2O_4 requires an increase in the heat-transfer rate in the evaporation zone by a factor 20 over the original value, which is not surprising. Firstly, the original value was derived from

the equation for convective heat transfer between a single-phase coolant and a grid matrix, whereas it is known that heat-transfer rates in boiling are substantially higher. Secondly, the cooled wall was made not of porous material but of a packet of thin sheets with spiral channels between them.

There are a few papers [17, 41] that deal with detailed theoretical [41] and experimental [17] researches, which are also compared. Lack of suitable data led the authors to calculate the heat-transfer coefficient for the evaporation zone as a superposition of the corresponding values for forced flow and bubble boiling in tubes. This mode of heat transfer persists until the critical difference between the saturation temperature and the temperature of the material is reached, which corresponds to the second critical heat flux during boiling. The scope for instability was not considered in the treatment, and a numerical technique was employed, which could not detect instability.

The observed and calculated temperature distributions within the porous wall agree satisfactorily while there are no deviations from the assumptions (Fig. 4), but the deviations under some circumstances cause liquid jets to break through.

Unexpected results were obtained on comparing the theoretical and observed pressure differences; the kinematic viscosity of a two-phase flow was calculated from (13), and it was observed that the calculated pressure difference was often more than ten times the measured value. Also, the effects of the position of the evaporation zone on the pressure difference were inverted: the calculated pressure difference for a constant flow rate increased as the evaporation zone moved towards the inner surface, whereas the measured difference showed the converse (Table 2).

A point here is that the capillary pressure $\Delta P = 2\sigma/r$ in these systems was close to the theoretical pressure difference, and therefore one can explain the quantitative and qualitative differences if one assumes that the effects from the capillary pressure increase as the evaporation zone approaches the inner wall. In that case, the capillary pressure distorts the results, so one cannot check the resistance calculations for two-phase flows.

Heat Transfer and Two-Phase Flow Structure in the Evaporation Zone. The evaporation zone has a decisive effect on the performance of a transpiration system, but measurements are difficult to make and virtually no reliable data are available on resistance and heat transfer during evaporation, so some conception of the process has to be derived from results for boiling under similar conditions. The most suitable data are those on boiling in capillaries, in thin films, and in porous materials coating continuous surfaces. For example, the internal diameters of the capillaries were d = 0.18-0.60 mm in the boiling measurements of [20-22, 45], and these are reasonably close to the mean pore size.

Boiling in a capillary is substantially different from boiling in a tube of macroscopic dimensions, because the internal diameter of a capillary is less than the capillary constant of the liquid $[\sigma/g(\rho_l - \rho_v)]^{1/2}$; the boiling of a flow in a capillary is of pulsating type. The liquid becomes heated as it moves, and it is superheated by an amount ΔT_0 at a certain distance from the inlet, at which point explosive bubble nucleation and growth occur. The large difference in specific volume between vapor and liquid results in the bubble filling the cross section almost instantly, which is followed by expansion towards the outlet, which expels the liquid. A reverse flow is also set up within the bulk of the liquid. The liquid plug becomes thinner as it is expelled on account of loss on the capillary walls, and the residual part is expelled from the mouth of the capillary. The very thin film left on the walls of the capillary evaporates very rapidly. Then a new bubble is formed and the process repeats. The exact period is governed by the time needed to produce a fresh bubble in the boiling region. The boiling mechanism is much the same for various liquids (water, ethanol, benzene, carbon tetrachloride, and nitrogen) and does not vary within the above range of capillary diameters.

Uniform heat production over the surface of the capillary by ohmic heating of the wall results in a distribution for the temperature difference $\Delta T = T_w - T_s$ along the length of the capillary, as ΔT increases along the region where the liquid is heated and superheated, with attainment of the maximum ΔT_0 at the start of boiling, which is followed by a fall in the region where the liquid film evaporates.

Attempts to increase the heat flux are restricted by the value at which random fluctuations in wall temperature occur near the exit from the capillaries, which is followed by the onset of a very rapid rise. This value for the heat flux is the critical value q*, and it can

be calculated from the heat-balance equation on the assumption that the liquid evaporates completely; the agreement with experiment is satisfactory [45]. A particularly important point is that q^* for boiling nitrogen attains the very high value of $q^* \approx 10^5$ W/m^2 [45], which is close to the first critical density for nitrogen boiling in large volumes.

This temperture pattern in the capillary walls and the very high heat-flux density are both due to the exceptionally rapid heat transfer in the boiling microfilm remaining on the channel walls: $q = \Delta T(\lambda'/\delta_{fi})$; it has been found [46, 47] that the critical heat-flux density for boiling in such films is several times that for bulk boiling under similar conditions. When the critical level is reached, the boiling microfilm contracts to a droplet that does not wet the surface. The corresponding wall superheating ΔT^* is substantially larger than that corresponding to the first boiling crisis in large volumes.

Evidence of the mechanism of evaporation in a porous material is provided by studies on the structure of two-phase air–water flows in straight and slightly curved flat channels of width 0.2-1.0 mm [48]; these studies revealed various features that distinguish a two-phase flow in a narrow slot from a flow in a channel of more ordinary size. For example, if the air and water flow rates are low in a curved channel of width 0.25 mm, the two-phase flow consists essentially of air separated by liquid plugs. The walls are coated by microfilms, whose minimum thickness is about 5 μm. These liquid plugs become thinner as the air speed increases, while the frequency of passage of the plugs increases. The air phase becomes continuous at higher speeds, and the surface of the film is covered by ripples, whose amplitude may vary in the range 20–40 μm.

Visual observations on the flow from porous materials can be used with researches on boiling and the motion of two-phase flows in capillaries in defining a mechanism for the evaporation. It must be pointed out that the mechanism itself is largely dependent on the characteristics of the heat input: bulk heat production or external surface input.

First we consider the model for bulk heat production, since this is closest to evaporation in capillaries with constant heat input.

A liquid flowing in a porous material with bulk heat production becomes heated, and the saturation point $t_s(P_l)$ is reached at a certain distance from the inlet, which corresponds to the local pressure; the temperature of the porous material then exceeds that of the coolant by ΔT_0, which is such that the first vapor bubbles appear (the numerical value of ΔT_0 is discussed below). The vapor is produced at isolated centers at the start of the evaporation region, and any bubble appearing at once fills the entire cross section, so the bubbles join up into large connected bubbles that fill the channels and emerge as jets. These jets may be separated by liquid plugs. The pressure pulsations set up by the bubbles cause local liquid flows that propagate in all directions, including transversely, although these flows are rapidly damped by narrow parts of the channels.

The number of nucleation centers increases as the flow moves onwards, and so does the number of vapor jets, so smaller and smaller channels become filled by vapor, and single jets are eventually replaced by a continuous vapor flow. The liquid plugs are broken up, and most of the liquid moves as a steadily thinning microfilm coating the particles and filling some pores. The speed of the vapor increases continuously. The channels are very variable in cross section and highly curved, so the vapor jets have considerable transverse motion, and vapor breaking through into pores filled with liquid produces minute droplets.

Ultimately, the microfilm dries up, and all the liquid plugs are distributed as minute droplets. The sharp changes in direction in the curvilinear channels cause the particles to strike the surfaces, so the droplets also rapidly vanish, and there is a fairly sharp end to the evaporation region.

The structure of the two-phase flow is decisive for the heat-transfer rate. The convective heat transfer in the single-phase part before the onset of boiling is replaced by thermal conduction via the microfilm, where the input heat supports the evaporation. The heat-transfer rate increases as the film becomes thinner, and therefore $T - t_s$ falls at the start of the evaporation region because the temperature of the porous material is reduced. The pressure in the flow falls as the two-phase mixture moves onwards, and therefore the saturation temperature also falls, so the liquid shows additional boiling and comes to a state of thermodynamic equilibrium. The temperature of the porous material then scarcely differs from the saturation temperature and also falls (Fig. 9a).

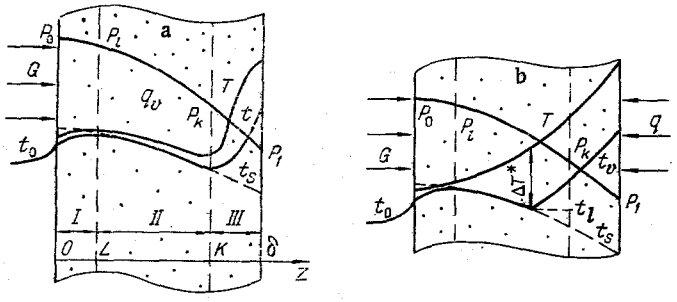

Fig. 9. Suggested physical models for liquid transpiration cooling: a) bulk heat production; b) external heat input; I) liquid flow; II) evaporation region; III) vapor flow.

There is extremely rapid heat transfer to the evaporating microfilm, simply on account of the very large specific surface area of the material, so one expects that all the liquid would evaporate under such conditions for any physically feasible bulk heat production rate. This is supported by one of the results of [15]: the temperature difference $T - t_s$ for a flowing two-phase mixture did not exceed 3-10°C for bulk heat production rates up to $q_v = 1.4 \cdot 10^9$ W/m^3. A possible restriction on the bulk heat production rate comes primarily from the thermal state of the vapor section, where the heat-transfer rates within the pores are much lower.

A more detailed study is required of the value of ΔT_0 at the start of the evaporation region. A standard analysis for bubble nucleation shows that bubbles arise primarily at areas of small-scale roughness on the surface. However, a porous material has an extremely complicated and extensive surface, which has a very marked influence on the behavior. Also, some of the vapor may remain within the connected channels after bubbles have appeared and vapor jets have escaped. This may result in continuous formation of vapor at numerous centers with a minimal value for ΔT_0 (in the quiescent state, without marked fluctuations).

These features are confirmed by measurements on the boiling in a porous material coating a solid surface. Visual observations reveal stable bubble boiling at pore mouths, while the superheating is much lower than that observed for smooth surfaces [49, 50]. The number of persistent centers in a porous coating is very substantial, while the bubbles are small. The initial superheating required to produce the boiling on porous coatings is less by a substantial factor than that for water on a smooth surface, e.g., values of 1-2°C apply for water boiling at atmospheric pressure [50, 51].

One therefore expects that the temperature of the porous material throughout the evaporation region would be within 1-5° of the local saturation temperature in bulk heat production (Fig. 9a).

The evaporation is entirely different for external heat input (Fig. 9b); here the heat is transferred by thermal conduction into the wall, and the temperature of the porous material rises continuously in the evaporation zone. When a certain critical temperature difference ΔT^* is reached, the liquid ceases to wet the material and the microfilm contracts to droplets. There is then a marked fall in the heat-transfer rate, and film evaporation gives way to convective heat transfer to a flow of superheated vapor containing minute droplets. These droplets do not wet the surface on collision, so they do not evaporate very rapidly, and some proportion of the liquid may emerge from the surface as the droplets.

Therefore, the temperature distribution in the evaporation zone should be described by two different equations, namely for the microfilm zone:

$$\lambda \frac{d^2T_2}{dZ^2} = h_1(T_2 - t_s), \quad T_2 - t_s < \Delta T^*, \tag{16}$$

and for the zone of superheated vapor of temperature t_v containing microdroplets:

$$\lambda \frac{d^2T_2}{dZ^2} = h_2(T_2 - t_v), \quad T_2 - t_v > \Delta T^*. \tag{17}$$

The heat-transfer rate h_2 can be calculated to a first approximation by means of (6) if a correction is applied for the presence and evaporation of the microdroplets.

Exact description of the heat transfer in the first zone requires the following parameters: the heat-transfer rate h_1 in microfilm evaporation and the critical temperature difference ΔT^*.

We can assume that h_1 is constant for the first zone, but the exact value remains an open question. An approximate expression is provided by the mean value of [15]:

$$\bar{h}_1 = \frac{q_v}{\Delta T} = \frac{9.25 \cdot 10^8}{6.5} = 1.43 \cdot 10^8 \text{ W/m}^3 \cdot \text{deg}.$$

We substitute the physical parameters of saturated steam at P = 1 bar; G = 0.6 kg/m^2·sec, $\beta/\alpha = 3.5 \cdot 10^{-6}$ m into (6) to get $h_V = 1.2 \cdot 10^6$ W/m^3·deg; this means that the heat-transfer rate for microfilm evaporation within a porous metal is about 100 times that for convective heat transfer within pores containing vapor. This result is in qualitative agreement with [26], where the factor was found to be 20.

The quantity $\Delta T^* = T^* - t_s$ is the critical superheating of the porous material in microfilm evaporation; the value may be estimated from the boiling of microfilms on solid surfaces [46, 47]. The boiling crisis in the microfilm is of thermodynamic origin, because the liquid becomes absolutely thermodynamically unstable and breaks up spontaneously. The corresponding limiting superheating is a physical characteristic of the liquid and can be calculated by reference to the mechanical stability of the homogeneous phase [52]. However, the limiting superheating of a liquid at a solid surface is substantially dependent on the effective surface tension, and therefore T* is always less than the analogous value for the pure liquid. Surface roughness and uncertainties over the physicochemical interaction result in indeterminacy in T* (the isothermal Leidenfrost temperature [53]) for various combinations of liquid and surface [47, 52, 53].

At a first approximation for ordinary conditions, we can calculate ΔT^* following the recommendations of [47]:

$$T^* - t_s = 0.83 \left(\frac{27}{32} T_{cr} - t_s \right). \tag{18}$$

Here T_{cr} is the thermodynamic critical temperature. One expects that ΔT^* for a liquid in a porous material will also be dependent on the structure of the material and on hydrodynamic effects arising from flow of the film and of the vapor.

Other Applications. Researches have been undertaken to expand the applications of liquid transpiration cooling beyond the classical systems of Fig. 1.

A description has been given [54] of a compact transpiration heat exchanger for disposing of waste heat under vacuum conditions. Countercurrent flows of heat and coolant are used in this device.

A preliminary analysis has been performed [55] of the scope for transpiration cooling in thermal stabilization of vessels containing cryogenic liquids under conditions of weightlessness.

Design and test data have been reported [56] for a porous cermet injector for a liquid rocket engine; two forms of injector were examined, in which the first had the components of the N_2O_4/MMH fuel mixing, evaporating, and beginning to react within the porous tungsten injector. In the second, the porous aluminum injector had only the N_2O_4 oxidant evaporating within it. Both designs provided good thermal protection of the injector by evaporation of the fuel components.

Conclusions. Theoretical and experimental researches have now defined the major features of liquid transpiration cooling; recent results have provided a reasonably good qualitative theory of the process that explains the instability and indicates methods of eliminating it. This method can serve as basis for extending measurements, which should be directed particularly to the following major and largely unexamined quantitative aspects:

1) resistance and heat transfer in the evaporation of a coolant in a porous material;

2) changes in the flow conditions in two-phase mixtures;

3) deviations from thermodynamic equilibrium in a two-phase evaporating flow; and

4) the effect of porous-material structure on the characteristics.

LITERATURE CITED

1. P. Grootenhuis, J. R. Aeron. Soc., 63, No. 578, 73 (1959).
2. V. A. Maiorov, Teplofiz. Vys. Temp. (1977) (paper deposited at VINITI, No. 1842-77, May 11, 1977).
3. V. A. Mairov and L. L. Vasil'ev, in: Acceleration of Heat and Matter Transport in Porous Media at Low Temperatures [in Russian], ITMO im. A. V. Lykova Akad. Nauk BSSR, Minsk (1975), p. 140.
4. V. A. Maiorov, Teploenergetika, No. 1, 64 (1978).
5. M. Jakob and I. B. Fieldhouse, Proceedings of the Second Symposium on Heat Transfer and Fluid Mechanics (1949), p. 191.
6. P. Duwez and H. L. Wheeler, J. Aeron. Sci., 15, No. 9, 509 (1948).
7. T. D. Hawkins, S. Hyman, C. Kuo, S. Israel, B. Minushkin, and M. Cooper, Transpiration and Film Cooling for Solid Propellant Rocket Nozzles, United Nuclear Corporation Report NDA 2150-1 (1961).
8. L. N. Bronskii and I. A. Zotikov, in: Physical Gas Dynamics, Heat Transfer, and Thermodynamics of Gases at High Temperatures [in Russian], Izd. Akad. Nauk SSSR (1962), p. 221.
9. P. N. Romanenko and Yu. P. Semenov, Heat and Mass Transfer [in Russian], Vol. 2, Nauka i Tekhnika, Minsk (1965), p. 280.
10. R. W. Evans, F. J. Crossland, and W. A. Baginski, IAAA Paper No. 65-290 (1965).
11. P. C. Wayner and S. G. Bankoff, AIChE J., 11, No. 1, 59 (1965).
12. V. K. Pai and S. G. Bankoff, AIChE J., 11, No. 1, 65 (1965).
13. V. K. Pai and S. G. Bankoff, AIChE J., 12, No. 4, 727 (1966).
14. J. C. Y. Koh and E. P. del Casal, Dev. Mech., 4, 1527 (1968).
15. V. M. Polyaev and A. V. Sukhov, Teplofiz. Vys. Temp., 7, No. 5, 1037 (1969).
16. J. C. Y. Koh, C. Jaeck, B. Benson, and B. Causineau, AIAA Paper No. 70-151 (1970).
17. R. Reth and W. Frost, AIAA Paper No. 72-25 (1972).
18. S. Kikawa and F. Chizaka, Bull. JSME, 15, No. 87, 1116 (1972).
19. V. M. Polyaev, É. V. Kharybin, and I. N. Bocharova, Teplofiz. Vys. Temp., 13, No. 1, 216 (1975).
20. E. W. Schwartz, ASME Paper No. 58-A-234 (1958).
21. V. A. Grigor'ev, A. G. Illarionov, V. I. Antipov, Yu. M. Pavlov, and A. S. Dudkevich, in: Papers from the Moscow Power Institute Conference on Researches during 1966-7, Commercial Heat Engineering Section, Drying and Heat-Exchanger Subsection [in Russian], Moscow (1967), p. 108.
22. D. A. Labuntsov, O. P. Evdokimov, I. V. Tishin, and A. F. Ul'yanov, Izv. Vyssh. Uchebn. Zaved. Mashinostr., No. 7, 68 (1970).
23. J. R. Schuster and T. G. Lee, AIAA Paper No. 72-389 (1972).
24. V. P. Popov and A. I. Shoikhet, in: Thermoaerodynamics [in Russian], ITMO Akad. Nauk BSSR, Minsk (1970), p. 17.
25. J. W. Yang, J. Spacecr. Rockets, 6, No. 6, 759 (1969).
26. Investigation of a Method for Transpiration Cooling of Liquid Rocket Chambers, NASA CR-107268, PWA-FR-3390 (1969).
27. N. D. Petrin, Izv. Vyssh. Uchebn. Zaved. Mashinostr., No. 7, 54 (1977).
28. A. Rubin and S. Schweitzer, Int. J. Heat Mass Transfer, 15, No. 1, 43 (1972).
29. V. A. Maiorov and L. L. Vasil'ev, Inzh.-Fiz. Zh., 24, No. 6, 1023 (1973).
30. V. A. Maiorov and L. L. Vasil'ev, Inzh.-Fiz. Zh., 25, No. 2, 237 (1973).
31. S. Schweitzer and D. Ronen, Heat Transfer 1974, 5, CT3.8, 113 (1974).
32. A. V. Luikov, L. L. Vasiliev, and V. A. Mayorov, Int. J. Heat Mass Transfer, 18, No. 7/8, 863 (1975).
33. A. V. Luikov, L. L. Vasiliev, and V. A. Mayorov, Int. J. Heat Mass Transfer, 18, No. 7/8, 885 (1975).
34. V. A. Maiorov, Inzh.-Fiz. Zh., 32, No. 5, 870 (1977).
35. V. A. Maiorov and L. L. Vasil'ev, in: Acceleration of Heat and Matter Transport in Porous Media at Low Temperatures [in Russian], ITMO im. A. V. Lykova Akad. Nauk BSSR (1975), p. 149.
36. V. A. Maiorov and L. L. Vasil'ev, in: Low-Temperature Heat-Tubes and Heat Exchangers [in Russian], ITMO im. A. V. Lykova Akad. Nauk BSSR, Minsk (1977), p. 3.
37. V. A. Maiorov and L. L. Vasil'ev, Vestsi Akad. Nauk BSSR, Ser. Fiz.-Energ. Navuk, No. 2, 104 (1977).
38. V. A. Maiorov and L. L. Vasil'ev, Vestsi Akad. Nauk BSSR, Ser. Fiz.-Energ. Navuk, No. 2, 112 (1977).

39. D. Moalem, Int. J. Heat Mass Transfer, 19, No. 5, 529 (1976).
40. D. Moalem and S. Cohen, Int. J. Heat Mass Transfer, 19, No. 12, 1415 (1976).
41. W. Frost, R. D. Reth, and W. T. Buchanan, AIAA Paper No. 72-24 (1972).
42. R. H. Boden, Trans. ASME, 73, No. 4, 385 (1951).
43. V. A. Maiorov and L. L. Vasil'ev, Vestsi Akad. Nauk BSSR, Ser. Fiz.-Energ. Navuk, No. 2, 112 (1978).
44. J. B. Kelley and M. R. L'Ecuyer, Transpiration Cooling — Its Theory and Application, JPC 422, Report No. TM-66-5 (1966).
45. V. A. Grigor'ev, V. I. Antipov, Yu. M. Pavlov, and A. V. Klimenko, Teploenergetika, No. 4, 11 (1977).
46. V. A. Grigor'ev, Yu. M. Pavlov, and E. V. Ametistov, Boiling of Cryogenic Liquids [in Russian], Énergiya, Moscow (1977).
47. I. A. Kopchikov, G. I. Voronin, T. A. Kolach, D. A. Labuntsov, and P. D. Lebedev, Int. J. Heat Mass Transfer, 12, No. 7, 791 (1969).
48. A. G. Beinusov, A. N. Khoze, and A. Ya. Cherkas, Izv. Akad. Nauk SSSR, Mekh. Zhidk. Gaza, No. 2, 170 (1978).
49. G. N. Danilova et al., in: Heat and Mass Transfer — V [in Russian], Vol. 3, Part 1 (1976), p. 22.
50. Abhat and Seban, Teploperedacha, Ser. C, 96, No. 3, 74 (1974).
51. G. F. Smirnov, Teploenergetika, No. 9, 77 (1977).
52. V. P. Skripov, in: Heat and Mass Transfer [in Russian], Vol. 2 (1962), p. 60.
53. Bomeister and Simon, Teploperedacha, Ser. C, 95, No. 2, 18 (1973).
54. O. G. Rasin and V. A. Krivonos, in: Acceleration of Heat and Matter Transport in Porous Media at Low Temperatures [in Russian], ITMO im. A. V. Lykova Akad. Nauk BSSR, Minsk (1975), p. 168.
55. Yu. I. Krokhin and A. S. Kulikov, Tr. Mosk. Eng. Inst., No. 198, 64 (1974).
56. J. Kahrs and A. D. Corbett, AIAA Paper No. 67-463 (1967).